Electronic Supplementary Material (ESI) for Nanoscale.

Supporting Information

Atomically Dispersed and Oxygen Deficient CuO Clusters as Extremely Efficient Heterogeneous Catalyst

Tingshi Zhang, ‡[a,b] Chengkai Yang, ‡[a,b] Borong Li,[a,b] Yuanming Zhang,[a,b] Zanyong Zhuang*[a,b] and YanYu *[a,b]

[a]College of Materials Science and Engineering, Fuzhou University, New Campus, Minhou, Fujian 350108, China

[b]Key Laboratory of Advanced Materials Technologies, Fuzhou University, Fujian 350108, China

*Corresponding author

E-mail: zyzhuang@fzu.edu.cn; yuyan@fzu.edu.cn.

(‡: These authors contributed equally to this work)

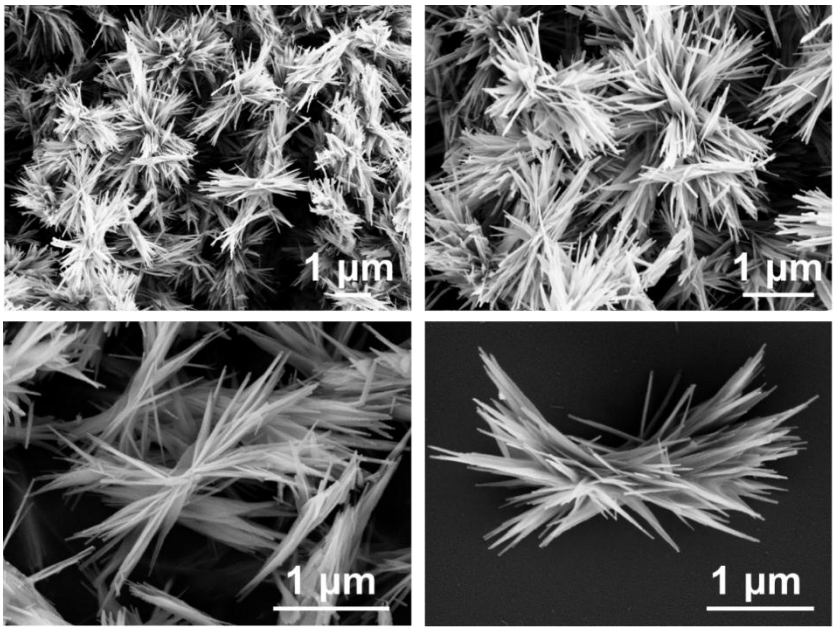

Fig. S1. The SEM images of CuO-AlOOH.

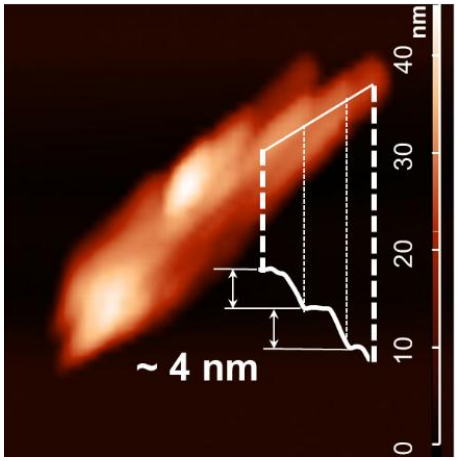

Fig. S2. (a, b) The XRD pattern and AFM image of CuO-AlOOH.

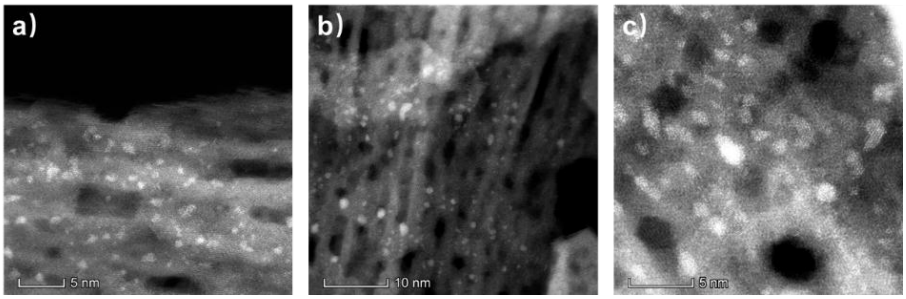

Fig. S3. The ACTEM images of CuO-AlOOH.

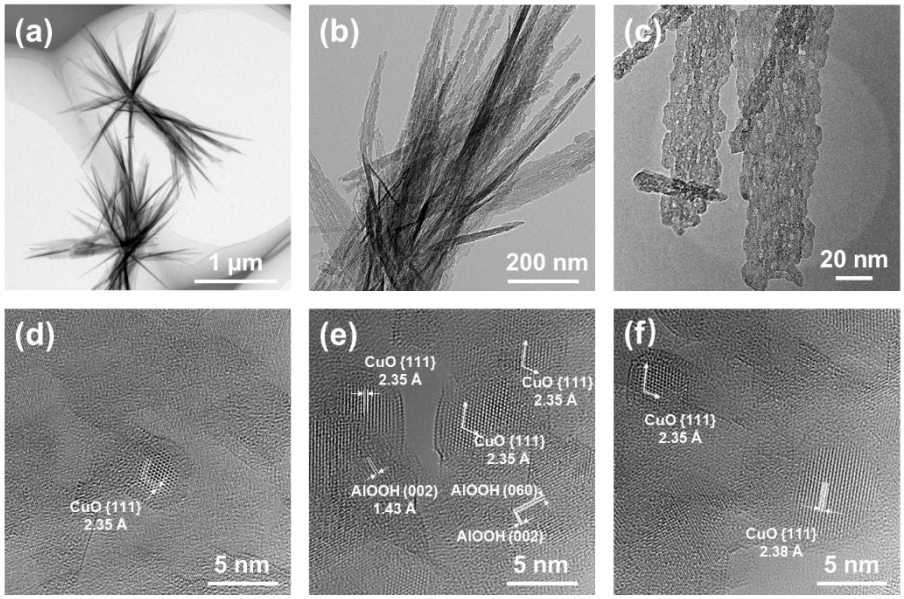

Fig. S4. The TEM images of CuO-AlOOH. These dots can be ascribed to CuO, displaying crossing lattice fringes with spacing of 0.235 nm and interfacial angle of about 70°, well matched the {111} facets of cubic CuO (JCPDS No.78-0428).

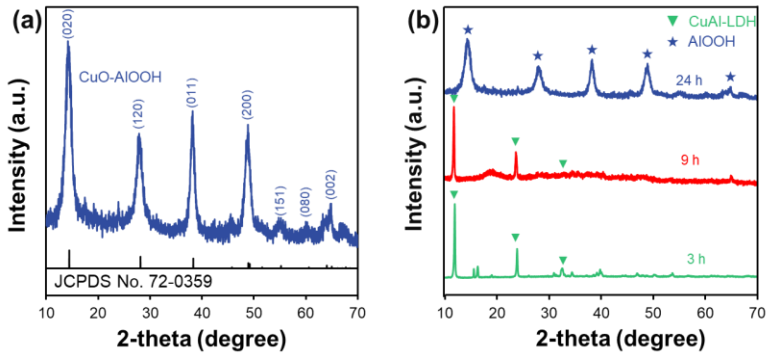

Fig. S5. (a) The XRD pattern of CuO-AlOOH, (b) XRD pattern of samples collected at different synthesis time.

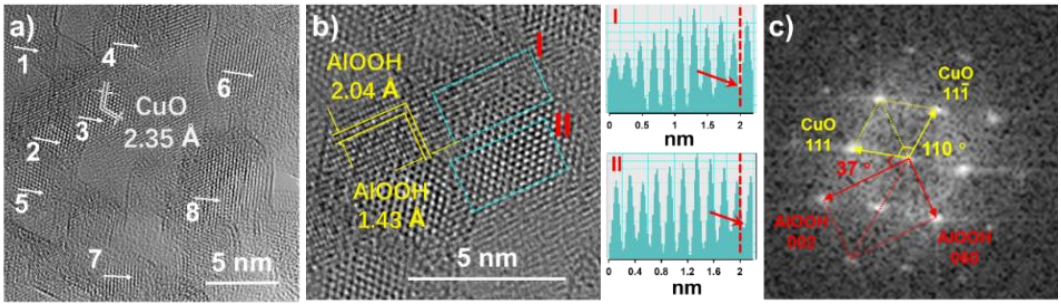

Fig. S6. a-b) HRTEM images of CuO-AlOOH, c) Fast Fourier transform (FFT) of the TEM image from a).

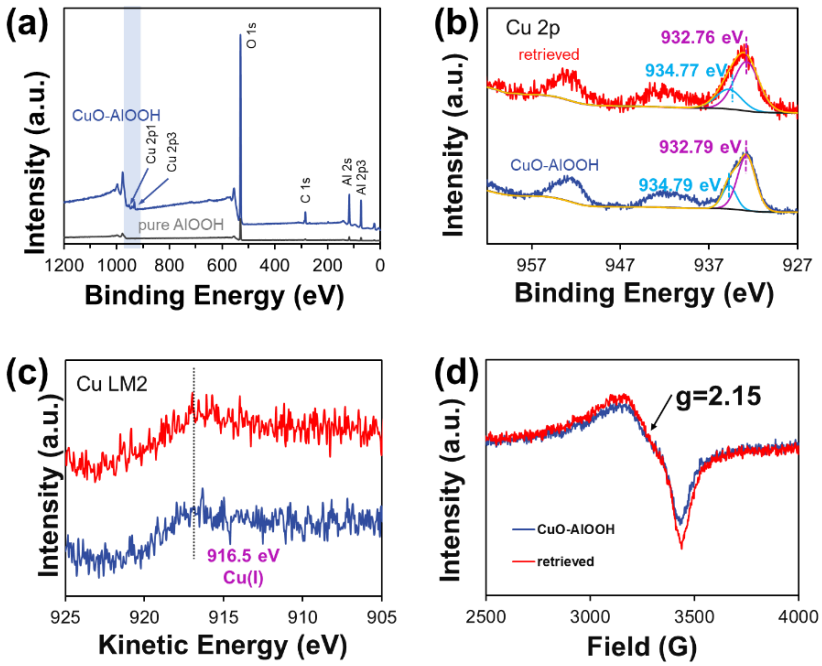

Fig. S7. (a) The XPS spectra of pure AlOOH and CuO-AlOOH, (b) Cu 2p XPS and (c) Cu LM2 spectra of CuO-AlOOH and retrieved CuO-AlOOH, (d) EPR spectra of CuO-AlOOH and retrieved CuO-AlOOH after catalytic reaction.

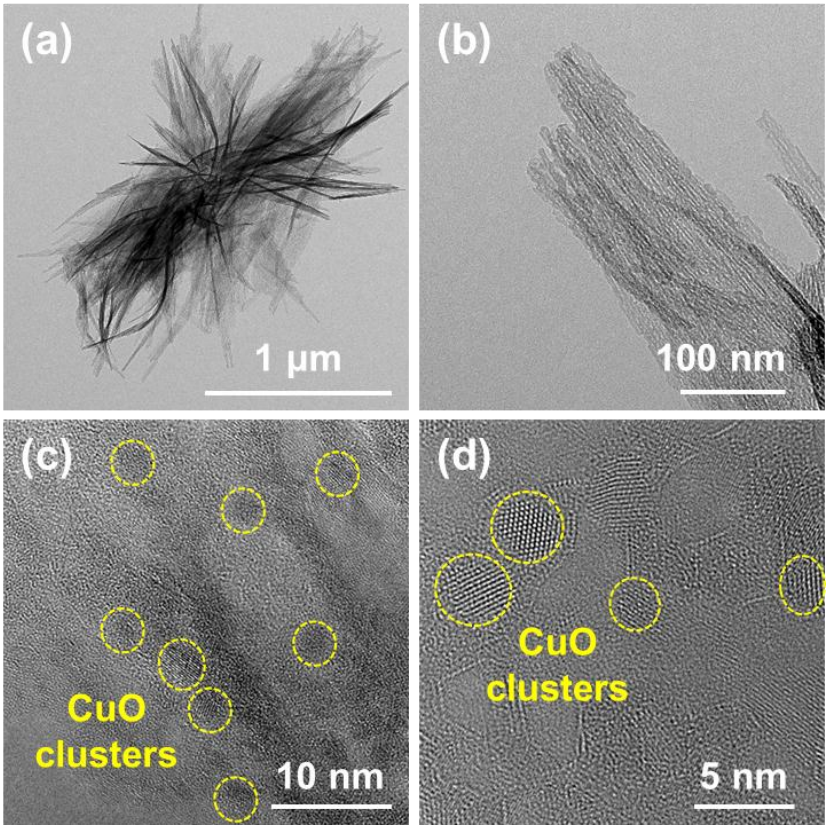

Fig. S8. TEM images of OVs-poor CuO/AlOOH.

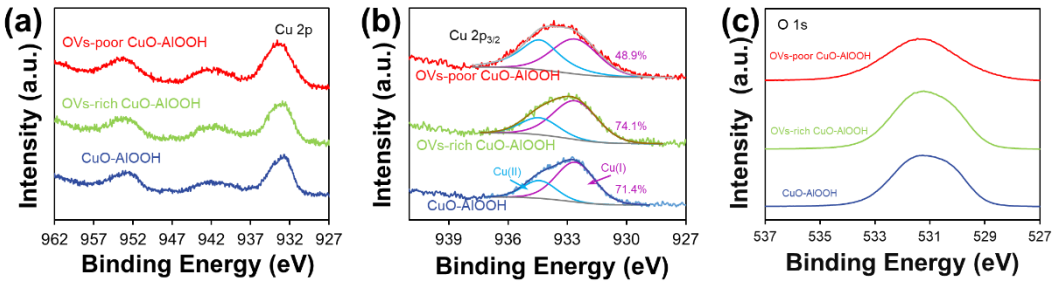

Fig. S9. (a, b) The Cu 2p, and (c) O1s XPS spectra spectra of CuO-AlOOH, OVs-rich CuO-AlOOH, OVs-poor CuO-AlOOH and mixture of CuO+AlOOH.

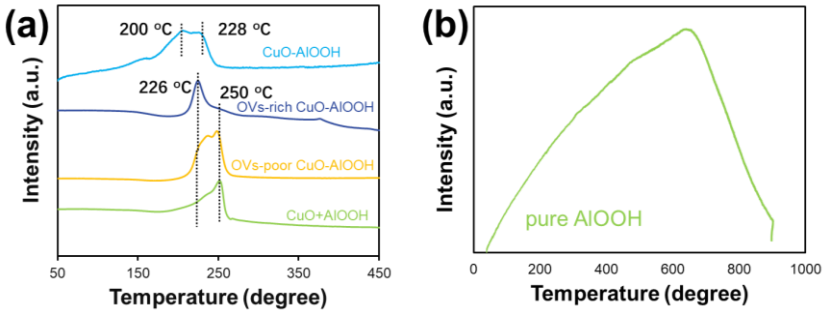

Fig. S10. H_2-TPR profiles of crude CuO-AlOOH, OVs-rich CuO-AlOOH, OVs-poor CuO-AlOOH, and the CuO+AlOOH reference.

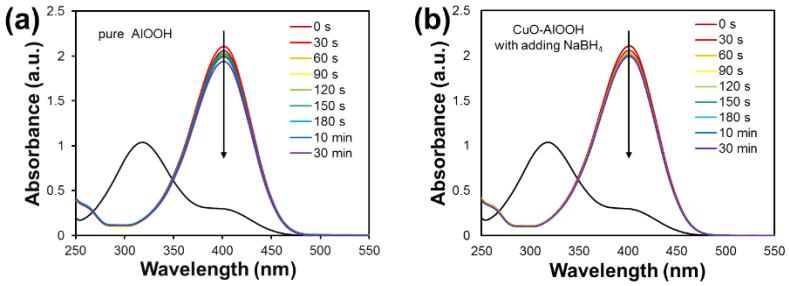

Fig. S11. Time-dependent UV–vis absorption spectra of 4-nitrophenol in presence of (a) pure AlOOH and (b) CuO-AlOOH without adding $NaBH_4$, respectively.

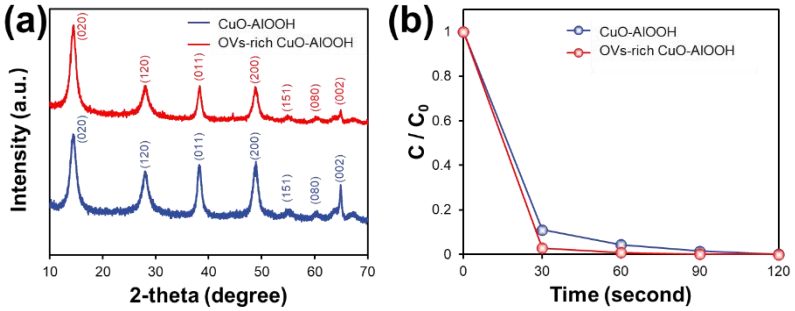

Fig. S12. (a) XRD patterns of CuO-AlOOH and CuO-AlOOH after annealed at 120 °C (denoted as OVs-rich CuO-AlOOH). (b) The catalyst activity of 4-NP reduction by using the CuO-AlOOH and OVs-rich CuO-AlOOH as the catalyst, respectively.

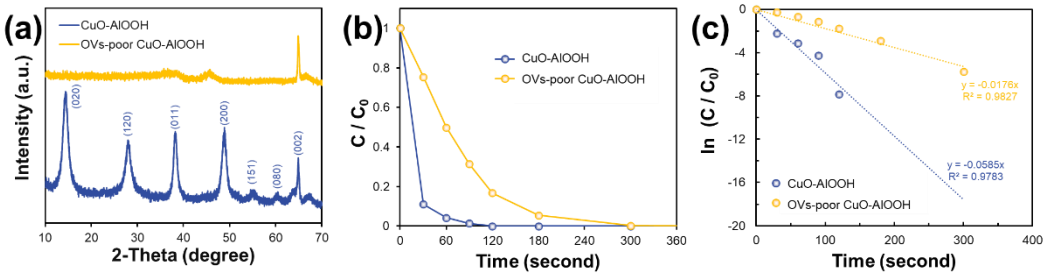

Fig. S13. (a) The XRD patterns of CuO-AlOOH and OVs-poor CuO-AlOOH. (b) The catalytic activity of 4-NP reduction by using CuO-AlOOH and OVs-poor CuO-AlOOH as catalyst, respectively. (c) Rate kinetics of 4-NP reduction by CuO-AlOOH and OVs-poor CuO-AlOOH.

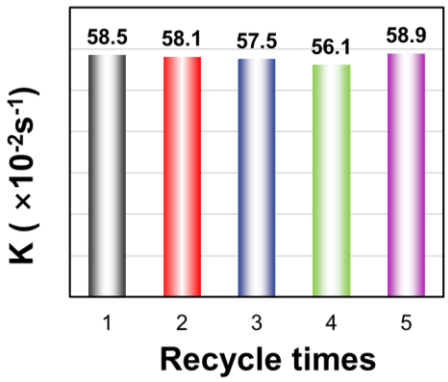

Fig. S14. Recyclability of CuO-AlOOH for 4-NP reduction.

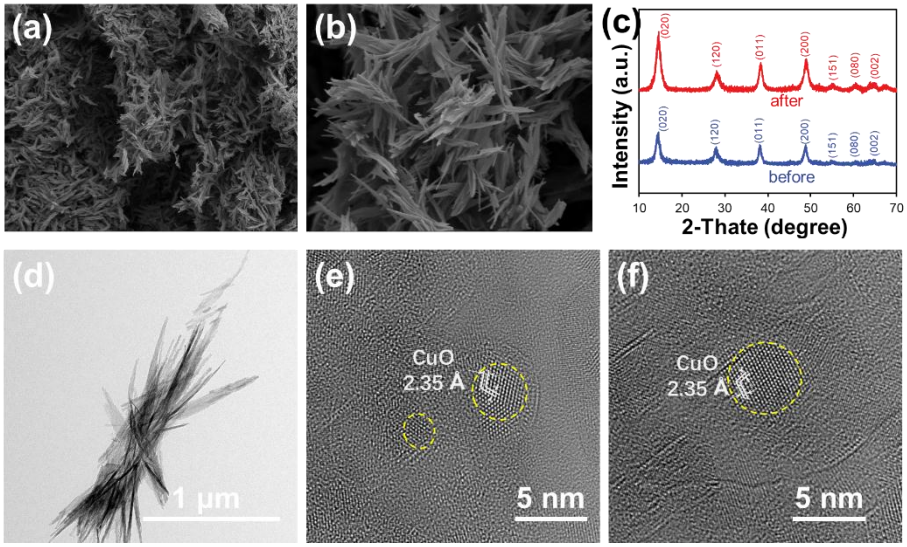

Figu. S15. (a, b) SEM images of retrieved CuO-AlOOH after the catalytic reaction. (c)The XRD patterns of CuO-AlOOH before and after the catalytic reaction. (d-f) TEM images of retrieved CuO-AlOOH after the catalytic reaction.

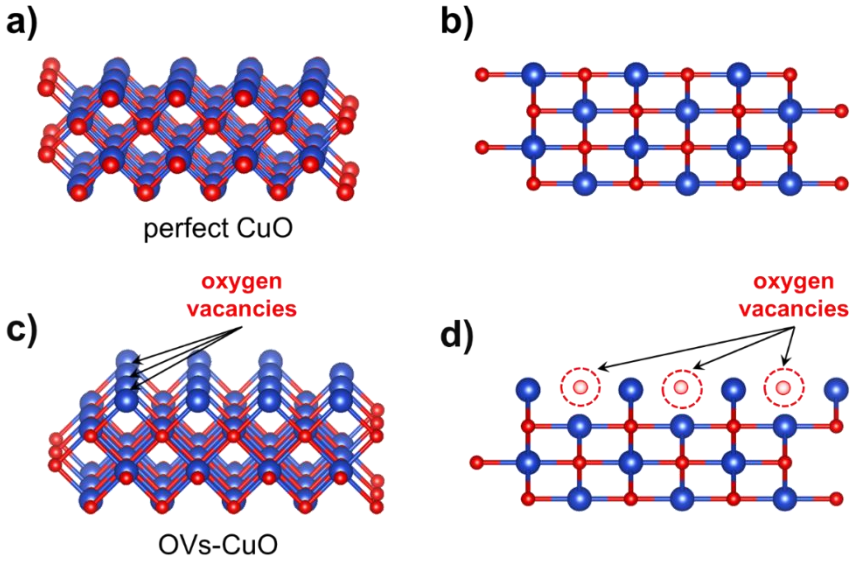

Fig. S16. (a, c) Front and (b, d) side view of perfect (a, b) CuO and (c, d) OVs-CuO atomic model.

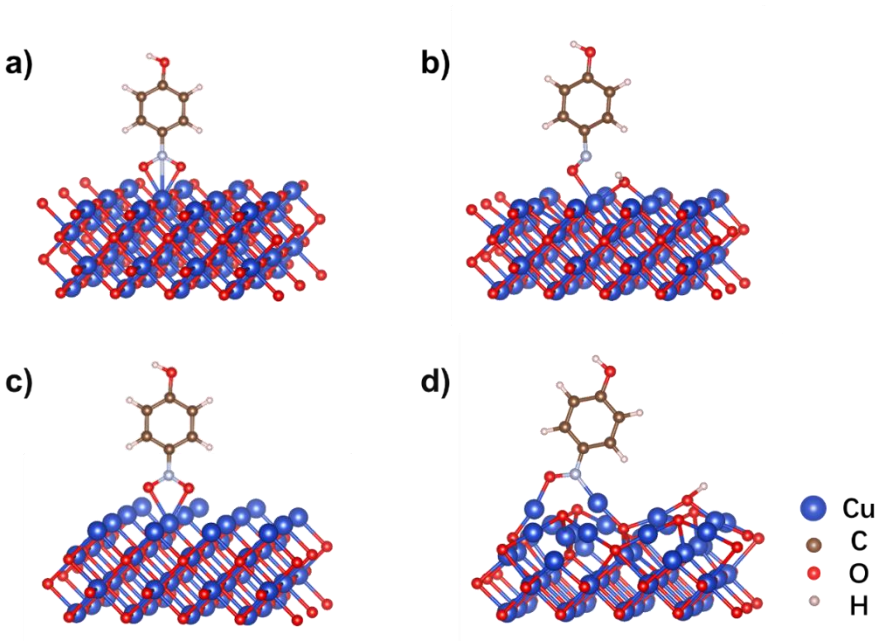

Fig. S17. (a) Atomic model of adsorption of 4-NP by perfect CuO. (b) The first hydrogenation step of 4-NP on perfect CuO. (c) Model of adsorption of 4-NP by OVs-CuO. (d) The first hydrogenation step of 4-NP on OVs-CuO.

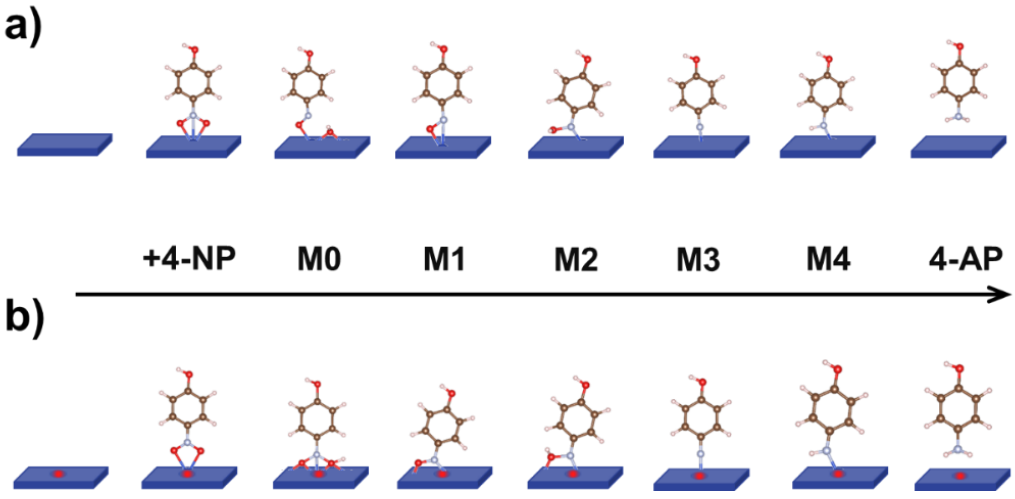

Fig. S18. Simplified model detail steps of adsorption and reduction of 4-NP by (a) perfect and (b) deficient CuO.